

This is a repository copy of *Direct Observation of Photochemical Free Radical Production from the Sunscreen 2-Phenylbenzimidazole-5-Sulfonic Acid via Laser-Interfaced Mass Spectrometry*.

White Rose Research Online URL for this paper:

<https://eprints.whiterose.ac.uk/150156/>

Version: Accepted Version

Article:

Wong, Natalie Gee Kwan, Berenbeim, Jacob and Dessent, Caroline Elizabeth Helen
orcid.org/0000-0003-4944-0413 (2019) Direct Observation of Photochemical Free Radical
Production from the Sunscreen 2-Phenylbenzimidazole-5-Sulfonic Acid via Laser-
Interfaced Mass Spectrometry. Chemphotochem. ISSN 2367-0932

<https://doi.org/10.1002/cptc.201900149>

Reuse

Items deposited in White Rose Research Online are protected by copyright, with all rights reserved unless indicated otherwise. They may be downloaded and/or printed for private study, or other acts as permitted by national copyright laws. The publisher or other rights holders may allow further reproduction and re-use of the full text version. This is indicated by the licence information on the White Rose Research Online record for the item.

Takedown

If you consider content in White Rose Research Online to be in breach of UK law, please notify us by emailing eprints@whiterose.ac.uk including the URL of the record and the reason for the withdrawal request.

Direct Observation of Photochemical Free Radical Production from the Sunscreen 2-Phenylbenzimidazole-5-Sulfonic Acid via Laser-Interfaced Mass Spectrometry

Natalie G. K. Wong, Dr. Jacob A. Berenbeim and Dr. Caroline E. H. Dessent*

Department of Chemistry, University of York, Heslington, York, YO10 5DD, U.K.

* Corresponding author: Email: caroline.dessent@york.ac.uk

Abstract

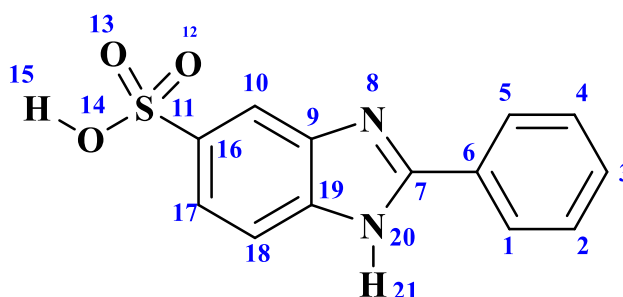
The common sunscreen molecule 2-phenylbenzimidazole-5-sulfonic acid (PBSA) is studied in its gas-phase deprotonated form ($[\text{PBSA-H}]^-$) for the first time as an important step in achieving a better understanding of its behavior as a photosensitizer. UV laser-interfaced mass spectrometry is employed, revealing that $[\text{PBSA-H}]^-$ photofragments into three ionic products (m/z 208, 193, and 80) with distinctive wavelength-dependent production profiles. Both the m/z 208 and 80 channels produce associated neutral free radical species. Collision-induced dissociation is performed on $[\text{PBSA-H}]^-$, showing that its hot ground-state dissociates only into m/z 193 (statistical fragment). Therefore, the m/z 208 and 80 fragments which are produced strongly through the UVA/UVB are characterized as non-statistical photofragments associated with non-ergodic excited-state decay. Our observation of non-statistical photofragments reveal that $[\text{PBSA-H}]^-$ is not behaving as a model sunscreen molecule. Further, our results indicate that the T_1 state, associated with photosensitization, decays with direct free radical production.

Keywords

Sunscreen, free radicals, laser spectroscopy, photolysis, photosensitizer.

1. Introduction

Sunscreens are widely employed to protect human skin from sunburn and the long-term consequences of exposure to the sun. The suitability of a given sunscreen molecule depends on a range of factors, but its effectiveness will clearly be limited if it behaves as a photosensitizer.^[1,2] (A photosensitizer is a molecule that subsequent to its activation by light, produces a chemical change in another molecule. Commonly, this involves generating reactive oxygen species that initiate further chemical reactions.) Surprisingly, several common organic sunscreen molecules (*e.g.* octocrylene, octylmethoxycinnamate, or oxybenzone) have been reported to enhance the production of reactive oxygen species.^[3-8] 2-phenylbenzimidazole-5-sulfonic acid (PBSA) is one such widely-used sunscreen (Scheme 1), which has been found to photogenerate reactive oxygen species and oxidize guanine residues *in cellulose* under UV radiation.^[9-11] There is currently a need to better understand the photosensitization mechanisms that occur for UV filters such as PBSA, in order to aid the rational development of future sunscreens.^[1,2]



Scheme 1. Schematic diagram of PBSA with atom labels.

In this paper, we adopt a new approach to better understand the photodegradation pathways and hence photosensitization mechanisms that are available to PBSA through applying the novel technique of laser-interfaced photodissociation mass spectrometry.^[12-14] PBSA exists as a deprotonated species, *i.e.* [PBSA-H]⁻, in solution due to the low pK_a of its sulfonic acid group. Here, we employ electrospray ionization to transfer [PBSA-H]⁻ from solution into the gas phase where the ion is then mass selected and interrogated with laser photons over a wide UV range. This allows us to monitor how the absorbance of the anion varies with wavelength, while simultaneously measuring the production of any photoproducts.^[12,13] Our laser-based approach is in the spirit of a number of recent studies where advanced spectroscopic techniques have been applied to sunscreen molecules under highly-controlled conditions.^[15-23]

Recent computational studies by Zhang *et al.* and Shen have been performed on PBSA to better understand its photophysical properties.^[24,25] Zhang *et al.* used density functional theory to assess the potential for triplet-state electron transfer from different protonation states of PBSA to triplet oxygen.^[24] They found that deprotonated PBSA could spontaneously transfer an electron to $^3\text{O}_2$ to generate reactive O_2^- , with the different protonation states varying in their propensity to effect electron transfer. Shen used time-dependent density functional theory to assess PBSA's photosensitizing potential, finding further evidence that singlet oxygen can be produced from the triplet excited state.^[25] To date, no computational studies have been performed to calculate the excited-state potential energy surfaces or direct photodegradation products. There have also been a number of solution-phase photochemical studies of PBSA, which have confirmed that the T_1 state can generate reactive oxygen species, and that their production is pH dependent.^[10,26–30] Experiments to track direct photodegradation products in solution are challenging due to secondary reactions and environmental effects. However, such measurements are important outside of the immediate interest in sunscreens, since these molecules are common aquatic pollutants, and a full understanding of potential photoproducts and their toxicity is crucial.^[26–30]

Gas-phase photochemical studies provide a complementary approach to mapping photodegradation where photoproducts can be directly identified, and experimental results can be straightforwardly compared to theoretical calculations. However, gas-phase laser spectroscopy of the ionic forms of sunscreen molecules are currently sparse,^[12,15] with only oxybenzone having been studied very recently in its protonated and deprotonated forms.^[15] Notably, deprotonated oxybenzone was observed to photofragment with production of methyl radicals in the UVB. This result is concerning as it adds to long-standing concerns that some sunscreens can produce free radicals following photoexcitation.^[19] In the current study on PBSA, we aim to better understand the generality of our recent oxybenzone results, as well as providing a more detailed insight into the photosensitizing behavior of PBSA.

Experimental and Computational Details

The gaseous ion absorption (photodepletion) and photofragment production spectra of [PBSA-H]⁺, were recorded *in vacuo* using action spectroscopy. An AmaZon SL mass spectrometer (Bruker Daltonics Inc., Billerica, MA, USA) modified for laser-interfaced mass spectrometry (LIMS), was used as described previously.^[12,13] PBSA was purchased from Sigma-Aldrich

(St. Louis, MA, USA) and used as received. HPLC-grade acetonitrile was purchased from Fisher Scientific, Inc. (Pittsburgh, PA, USA). PBSA solutions (1×10^{-5} mol dm⁻³ in CH₃CN) were electrosprayed at a capillary temperature 160 °C.

[PBSA-H]⁻ was mass selected (*m/z* 273) and isolated in the ion trap prior to laser irradiation. Photons were produced by an Nd:YAG pumped OPO laser (Surelite™/Horizon™, Amplitude Laser Group, San Jose, CA, USA), giving $0.3 \pm 10\%$ mJ across the range 500-216 nm (2.48-5.74 eV), with 2 nm laser step sizes. Photofragmentation experiments were conducted with an ion accumulation time of 10 ms. To minimize the possibility of multiphoton events via sequential absorption, each mass-selected ion packet interacts with only one laser pulse (fragmentation time of 100 ms), and photodepletion restricted to ~40% of the precursor ion at the wavelength of maximum absorption. Multiphoton events via instantaneous absorption of multiple photons in the Frank-Condon region are negligible as the laser beam is only softly focused through the ion-trap region. Photodepletion (PD) of [PBSA-H]⁻ was measured as a function of the scanned wavelength, with photofragment production (PF) recorded simultaneously:

$$\text{Photodepletion Intensity} = \frac{\ln\left(\frac{\text{Int}_{\text{OFF}}}{\text{Int}_{\text{ON}}}\right)}{\lambda \times P} \quad [1a]$$

$$\text{Photofragmentation Intensity} = \frac{\left(\frac{\text{Int}_{\text{FRAG}}}{\text{Int}_{\text{OFF}}}\right)}{\lambda \times P} \quad [1b]$$

$$\text{Relative Ion Yield} = \text{Int}_{\text{FRAG}} / \text{Int}_{\text{PFT}} \quad [1c]$$

In these expressions, Int_{OFF} and Int_{ON} are the laser off and on parent ion peak intensities respectively; Int_{FRAG} is the fragment intensity with the laser on; λ is the excitation wavelength (nm); P is the laser pulse energy (mJ); and Int_{PFT} is the sum of the photofragment ion intensities with the laser on. The photodepletion spectrum is considered to be equivalent to the gaseous absorption spectrum in the limit where excited state fluorescence is negligible.^[13,14,31]

Photodepletion intensities were taken from an average of three runs at each wavelength of the range studied. We note that fragment ions with *m/z* < 50 are not detectable in our mass spectrometer since low masses fall outside the ion-trap mass-window.

Higher-energy collisional dissociation (HCD) was performed to investigate the ground-state thermal fragmentation characteristics of [PBSA-H]⁻, using an Orbitrap™ Fusion Tribrid mass spectrometer (Thermo Fisher Scientific, Waltham, MA, U.S.A.) as described previously.^[32,33] Solution-phase UV-VIS absorption spectra of PBSA (aqueous solution; 3×10^{-5} mol dm⁻³)

were recorded with a UV-1800 spectrophotometer (Shimadzu, Kyoto, Japan) with a 10 mm UV quartz cuvette, with deionized H₂O as the baseline solvent.

All calculations were performed using Density Functional Theory (DFT) at the B3LYP/6-31+G** level in Gaussian 09.^[34] The bulk solvent effect of CH₃CN was considered by using the integral equation formalism polarized continuum model (IEFPCM) based on the self-consistent-reaction-field (SCRF) method. All reported structures correspond to true minima, as confirmed by frequency calculations.

2. Results and Discussion

2.1 Identification of the Deprotonation Site in [PBSA-H]⁻ via Density Functional Theory Calculations

The sulfonic acid group is a strongly acidic group, so PBSA will be deprotonated at the **H15** position (Scheme 1) in aqueous solution to form the sulfonate monoanion.^[29] Deprotonation is also possible from the **H21** position at higher pH.^[29] Relative energies of the two deprotomers of [PBSA-H]⁻ were calculated in the gas phase and in acetonitrile to reveal which deprotomer or deprotomer(s) will be produced following electrospray (Table 1). (Electrospray does not always transfer the most stable solution-phase ion to the gas phase).^[12,35,36] In the subsequent discussion, we label the two possible deprotomers as **O14** and **N20** in line with the excess negative-charge site.

As expected, deprotonation is favored from the sulfonic acid group (**O14**), both in the gas phase and in acetonitrile, although the relative energies of the two deprotomers are closer in the gas phase. Boltzmann population calculations indicate that the **O14** deprotomer dominates (>99.9%) in acetonitrile at 458 K. Since electrospray from acetonitrile solutions maintains the solution-phase ratios of different tautomeric species,^[12,35] we expect the **O14** deprotomer to almost entirely dominate the gaseous ion population. Vertical detachment energies (VDE) of the gaseous deprotomers are also listed in Table 1.

2.2 UV Absorption Spectra of [PBSA-H]⁻: Gas Phase versus Solution Phase

Figure 1 shows the electrospray ionization mass spectrum obtained when a solution of PBSA in acetonitrile is sprayed in negative ion mode, showing [PBSA-H]⁻ (m/z 273) as the dominant

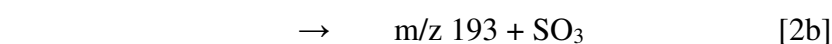
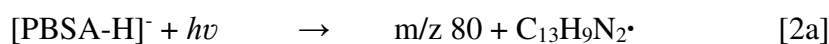
peak. The gas-phase absorption spectrum of mass-selected [PBSA-H]⁻ across the 2.48-5.74 eV (500-216 nm) range, recorded *via* photodepletion, is shown in Figure 2a. Mass selection is a key advantage of the experimental approach we employ here as it allows us to directly probe the intrinsic properties of the [PBSA-H]⁻ anion.

The gaseous absorption spectrum of [PBSA-H]⁻ displays strong absorption in the UVA region (with an absorption onset around 3.40 eV) through a band which then reduces in intensity through the UVB range. Absorption again increases to higher energies through the UVC region. To aid discussion of the photofragment production spectra (see Section 2.3), the photodepletion spectrum has been labelled as being composed of features **I-IV**, with **I** representing the strong UVA-UVB band. Figure 2b presents an aqueous absorption spectrum of PBSA (pH 7.1) obtained as part of this work for direct comparison with the gas-phase absorption spectrum. The spectrum agrees well with previously-published ones.^[5,11,26-29] Comparing the gaseous and solution-phase spectra, feature **I** can be seen to blue-shift significantly on going from the gas-phase to solution (band maxima at ~340 nm versus 315 nm), a trend which is consistent with the transition displaying charge-transfer character where the excess charge is more localized in the initial ion than in the excited state.^[37]

Given that the calculated VDE of the **O14** deprotomer is 4.39 eV, we predict that band **I** exists within the bound (non-electron-detached) region for this anionic species. Electronic excitations lying above this energy occur within the electron detachment continuum, so that any gas-phase photoexcitation above 4.39 eV is likely to be accompanied by electron detachment.^[38]

2.3 Photofragmentation of [PBSA-H]⁻

We next turn to exploring the photofragment ions that are associated with the excited states evident in the Figure 2a spectrum. Figure 3 displays the difference (laser on - laser off) photofragment mass spectra of [PBSA-H]⁻ irradiated at the photoabsorption maxima of features **I-IV** (3.8, 4.5, 4.9, and 5.3 eV, respectively). Photofragmentation produces *m/z* 80, 193, and 208 as the dominant ionic products, with equations [2a]-[2c] illustrating the fragmentation pathways associated with their production:



176 \rightarrow m/z 208 + HSO₂[•] [2c]

177 Table 2 lists the proposed structures of the ionic photofragments and their accompanying
178 neutral fragments. Inspection of the structures shown in Table 2 reveals that
179 photofragmentation is localized around the **S11-C16** bond, with pathways [2a] and [2b] arising
180 from the fission of this bond with the excess charge moving in two different directions.
181 Photofragment m/z 208 is produced *via* a less direct pathway, which involves intramolecular
182 rearrangement to eject the HSO₂[•] neutral. We note that the structures of the lower mass
183 fragments mean that these ions cannot be produced through fragmentation of higher mass ions,
184 ruling out the possibility that they are produced through a sequential multiphoton processes.
185 The key point of note about the photofragment pathways, is that two of these pathways ([2a]
186 and [2c]) result in the production of free-radical species.

187 To provide further insight into the nature of the [PBSA-H]⁻ excited states and decay pathways,
188 Figures 4b-4d present the production spectra for the three ionic photofragments m/z 80, 193,
189 and 208, with the parent [PBSA-H]⁻ photodepletion spectrum displayed again in Figure 4a for
190 ease of comparison. The photofragment production spectra highlight that all of the
191 photofragments are produced to some extent across the entire photoexcitation range from 3.40-
192 5.74 eV.

193 The action spectrum of the lowest mass ionic photofragment, m/z 80, is shown in Figure 4b
194 and is very similar to the [PBSA-H]⁻ gaseous absorption spectrum. This is also largely true for
195 the m/z 208 photofragment (Figure 4d), although this photofragment is produced more weakly
196 across the high-energy **III/IV** regions. The profile of the high-energy spectral range for the m/z
197 208 photofragment is similar to other photofragment spectra we have recorded previously,
198 where a higher-mass photofragment dissociates into a lower-mass photofragment at high
199 internal excitation energy.^[12]

200 Figure 4c displays the photoproduction spectrum of the most intense ionic photofragment
201 (m/z 193), which is notable compared to the other two photofragments as it is produced much
202 less strongly through region **I**, with intensity subsequently increasing with excitation
203 wavelength into the UVC region.

204 It is evident from the data presented in Figures 3 and 4 that the relative production of the three
205 observed photofragments from [PSBA-H]⁻ varies significantly as a function of photon energy.
206 Figure 5 presents a plot of the relative ion yield of the photofragments, providing a concise
207 overview of photofragment production. Within the UVA region (3.5-4.1 eV), the relative ion

yields of the m/z 80 and 208 photofragments are larger than that of the m/z 193 ion. At photon energies above 4.1 eV, however, production of the m/z 193 fragment increases strongly, with relative production peaking around 4.5 eV. These results are discussed in the context of PBSA's ability to act as an efficient UV filter in the next section.

Electron loss is a dominant photofragmentation channel for [PBSA-H]⁻ as for other gaseous anions we have studied,^[15, 38] *i.e.*



Section S2 of the Supporting Information provides an electron detachment yield spectrum, and further details of the extent of electron detachment versus ionic fragmentation. At 224 nm, for example, electron detachment is estimated to constitute 85% of photodepletion compared to 15% branching into ionic fragments. Despite the strong propensity for electron detachment in the gas-phase, it is well established that the propensity of an anionic molecule to photodetach will be quenched upon solvation,^[39] so simple electron detachment is likely to be a less important channel compared to ionic fragmentation in solution.

2.4 Thermal Fragmentation versus Photofragmentation

To act as an efficient sunscreen, a molecule must be able to convert the harmful UV radiation it has absorbed into benign thermal energy. This is achieved by the electronic excited state(s) being able to rapidly relax back to the electronic ground state from where excess energy is dissipated by heat loss.^[1,2] In solution, this thermal energy can be lost to the bulk solvent *via* vibrational relaxation, but in the gas phase, this energy is conserved within the molecular system and the ensuing hot ground state will dissociate across the available fragmentation barriers which are the same as those that are available to the isolated molecule when it is heated (so called "statistical fragmentation"). For molecular ions, a closely comparable "heating" process occurs in collision-induced dissociation.^[40] [PBSA-H]⁻ was therefore subjected to collisional excitation to allow the fragmentation pathways associated with hot ground-state fragmentation to be identified.

Figure 6 displays the higher-energy collisional dissociation (HCD) fragmentation curves for [PBSA-H]⁻. Collisional activation reveals that the m/z 193 molecular ion completely dominates the thermal fragmentation profile of [PBSA-H]⁻, with the m/z 80 and 208 fragments only being seen as extremely minor fragments at the very highest collisional energies

(>50%).^[41] We can therefore conclude that statistical fragmentation of [PBSA-H]⁻ would proceed with production of only the m/z 193 fragment (pathway [2b]).

The relative ion yield plots shown in Figure 5 are clearly not consistent with a picture where UVA/UVB excitation of isolated [PBSA-H]⁻ leads to the ultrafast decay back to the electronic ground state, followed by statistical fragmentation solely into the m/z 193 fragment. (If this was the case, we would expect to see m/z 193 as the only photofragment with an ion yield profile that follows the absorption spectrum.) Instead, photoexcitation across the UV leads to strong production of the non-statistical fragments (m/z 80 and 208). Such non-statistical (or non-ergodic) processes occur when dissociation proceeds directly from the excited state without significant adiabatic conical-intersection involvement to return the system back to the ground state in the vicinity of the initial geometry.^[42] This is particularly true in the UVA region where the m/z 193 fragment is the minor fragment, indicating non-statistical excited state decay dominates.

The ion-yield plots displayed in Figure 5 show that statistical dissociation, i.e. dissociation into m/z 193, is enhanced in the UVC region < 280 nm. For deprotonated PBSA as well as neutral PBSA, there are currently no calculations of the excited state potential energy surfaces, so the molecular mechanism that precedes statistical decay is currently unknown. From precedents in other organic molecular systems, it is likely that this could be mediated by a conical intersection involving a bond rotation of the bridging C-C linking the imidazole and benzene,^[43] although it is also possible a conical intersection could be reached may be rotation of the sulfonate group to the imidazole instead. Calculations of the excited state surfaces are highly desirable to provide further insight into the mechanism(s) involved.^[43]

2.5 Implications of the Gas-Phase Results for Solution-Phase Photochemistry

The most detailed solution-phase study of PBSA photochemistry and photophysics conducted to date was that of Inbaraj et al.^[10] Measurements included the determination of the UVB quantum yield for production of singlet oxygen from deprotonated PBSA (0.05 in D₂O), as well as the fluorescence quantum yield (0.63). They noted that phosphorescence was also detected, although no quantum yield for this channel was reported. Importantly, the T₁ triplet excited state was found to be sufficiently long-lived at 77K for the characteristic electron paramagnetic resonance half-field transition to be detectable. No photofragmentation quantum yields were reported in the study.

It is important at this point to consider how our gas-phase results relate to the photochemistry of PBSA in solution. In Section 2.2, we noted that the region **I** absorption blue-shifts upon solvation. It is reasonable to assume that the photochemistry we observe across region **I** in the gas-phase (3.4-4.2 eV), similarly blue-shifts in solution to the 3.8-4.6 eV range. Zhang *et al.* has calculated the solution-phase S_1 excitation energy of $[\text{PBSA-H}]^-$ as 4.045 eV,^[24] an energy which lies in region **I** (solvated). By analogy, we expect that the S_1 state is reached through gas-phase region **I** in our experiment. This state is important as it is believed to act as a doorway to the long-lived T_1 state.^[24] It is notable that the strong production of non-statistical photofragments associated with pathways [2a] and [2c] occurs through region **I**, leading us to conclude that these are the direct photodegradation products of the T_1 state.^[24,25,29] Similarly, since the T_1 state has been previously attributed with leading to PBSA's behavior as a photosensitizer,^[24,25,29] our results suggest that photosensitization by PBSA in solution is not simply associated with electron and energy transfer from the T_1 state, but also through direct formation of free radical products. We note that geminate recombination of any free radical photoproducts may occur in solution, and it will be important in future solution-phase measurements to directly explore whether these direct free radical products can be detected, for example by employing techniques such as spin trapping.^[44]

3. Concluding Remarks

In summary, we report for the first time the gaseous electronic photoabsorption spectrum and direct photofragment production profile spectra of the native form of PBSA, a popular FDA-approved UV filter found within many existing commercial sunscreens. The novelty of our gas-phase experiment is that it allows us to map the direct laser-induced photodegradation products of $[\text{PBSA-H}]^-$, away from the complications of bulk mixtures where secondary photoproducts can dominate. Strikingly, we observe evidence for high-yield production of free-radical species at photon energies between 3.5-5.5 eV. $[\text{PBSA-H}]^-$ is observed to largely photodissociate primarily *via* the heterolytic cleavage of the **S11-C13** bond (pathway [2b]); however, competitive homolytic dissociation yielding odd-electron products (pathways [2a] and [2c]) is seen strongly across UVA/UVB absorbance wavelengths. By comparing our gaseous spectra with the solution-phase absorption spectrum, we conclude that the non-statistical odd-electron photofragments (pathways [2a] and [2c]) are the direct photodegradation products of the T_1 state. Indeed, the long-range repulsive interaction inherent

in the triplet state is known to aid in the breakdown of such states into such free radical pairs.^[45]
The identification of the direct photoproducts in this work is important as it can guide detection
of the direct photolysis products in future condensed-phase studies, as well as informing
assessment of the possible toxicity of photoproducts. Furthermore, our results indicate that
future theoretical studies (which are generally performed on gaseous molecules initially)
should include this direct photodegradation pathway to provide a more complete understanding
of the photosensitizing behavior of PBSA. Such work is highly desirable to guide the rational
development of improved UV filters.^[43,46]

Acknowledgements

This work was funded through the Leverhulme Trust Research Project Grant RPG-2017-147.
We thank the University of York and the Department of Chemistry for provision of funds for
the OPO laser system. We are grateful for computational support from the University of York
High Performance Computing service, Viking and the Research Computing team. The York
Centre of Excellence in Mass Spectrometry, used for the higher-energy collisional dissociation
(HCD) work, was created thanks to a major capital investment through Science City York,
supported by Yorkshire Forward with funds from the Northern Way Initiative, and
subsequently received additional support from the EPSRC. We also thank Mathew Hawkrige
for early contributions to this work.

Conflict of Interest

The authors declare no conflict of interest.

References

- [1] S. Forestier, *J. Am. Acad. Dermatol.* **2008**, *58*, S133-8.
- [2] F. Gasparro, *Sunscreen Photobiology*, Springer, Berlin, **1997**.
- [3] K. M. Hanson, E. Gratton, C. J. Bardeen, *Free Radic. Biol. Med.* **2006**, *41*, 1205–1212.
- [4] V. Brezová, S. Gabčová, D. Dvoranová, A. Staško, *J. Photochem. Photobiol. B Biol.* **2005**, *79*, 121–134.
- [5] N. Serpone, A. Salinaro, A. V. Emeline, S. Horikoshi, H. Hidaka, J. Zhao, *Photochem. Photobiol. Sci.* **2002**, *1*, 970–981.
- [6] P. J. McHugh, J. Knowland, *Photochem. Photobiol.* **1997**, *66*, 276–81.
- [7] J. M. Allen, C. J. Gossett, S. K. Allen, *Chem. Res. Toxicol.* **1996**, *9*, 605–609.
- [8] J. Knowland, E. A. McKenzie, P. J. McHugh, N. A. Cridland, *FEBS Lett.* **1993**, *324*, 309–313.
- [9] N. Bastien, J.-F. Millau, M. Rouabhia, R. J. H. Davies, R. Drouin, *J. Invest. Dermatol.* **2010**, *130*, 2463–2471.
- [10] J. J. Inbaraj, P. Bilski, C. F. Chignell, *Photochem. Photobiol.* **2002**, *75*, 107–16.
- [11] C. Stevenson, R. J. H. Davies, *Chem. Res. Toxicol.* **1999**, *12*, 38–45.
- [12] E. Matthews, C. E. H. Dessent, *Phys. Chem. Chem. Phys.* **2017**, *19*, 17434–17440.
- [13] E. Matthews, A. Sen, N. Yoshikawa, E. Bergström, C. E. H. Dessent, *Phys. Chem. Chem. Phys.* **2016**, *18*, 15143–15152.
- [14] R. Antoine and P. Dugourd, *Phys. Chem. Chem. Phys.* **2011**, *13*, 16494–16509.
- [15] N. G. K. Wong, J. A. Berenbeim, M. Hawkrige, E. Matthews, C. E. H. Dessent, *Phys. Chem. Chem. Phys.* **2019**, *21*, 14311–14321.
- [16] N. D. N. Rodrigues, N. C. Cole-Filipiak, M. A. P. Turner, K. Krokidi, G. L. Thornton, G. W. Richings, N. D. M. Hine, V. G. Stavros, *Chem. Phys.* **2018**, *515*, 596–602.
- [17] L. A. Baker, M. Staniforth, A. L. Flourat, F. Allais, V. G. Stavros, *ChemPhotoChem* **2018**, *2*, 743–748.
- [18] C. Ma, C. T. L. Chan, R. C. T. Chan, A. K. W. Wong, B. P. Y. Chung, W. M. Kwok, *Phys. Chem. Chem. Phys.* **2018**, *20*, 24796–24806.
- [19] M. T. Ignasiak, C. Houee-Levin, G. Kciuk, B. Marciniak, T. Pedzinski, C. Houée-Levin, G. Kciuk, B. Marciniak, T. Pedzinski, *ChemPhysChem* **2015**, *16*, 628–633.
- [20] S. Wang, S. Schatz, M. C. Stuhldreier, H. Böhnke, J. Wiese, C. Schröder, T. Raeker, B. Hartke, J. K. Keppler, K. Schwarz, et al., *Phys. Chem. Chem. Phys.* **2017**, *19*, 30683–30694.

- 361 [21] E. M. M. Tan, M. Hilbers, W. J. Buma, *J. Phys. Chem. Lett.* **2014**, 5, 2464–2468.
- 362 [22] J. C. Dean, R. Kusaka, P. S. Walsh, F. Allais, T. S. Zwier, *J. Am. Chem. Soc.* **2014**,
363 136, 14780–14795.
- 364 [23] M.-O. Winghart, J.-P. Yang, M. Kuhn, A.-N. Unterreiner, T. J. A. Wolf, P. D. Dau,
365 H.-T. Liu, D.-L. Huang, W. Klopper, L.-S. Wang and M. M. Kappes, *Phys. Chem.*
366 *Chem. Phys.* **2013**, 15, 6726–6736.
- 367 [24] S. Zhang, J. Chen, X. Qiao, L. Ge, X. Cai, G. Na, *Environ. Sci. Technol.* **2010**, 44,
368 7484–7490.
- 369 [25] L. Shen, *Spectrochim. Acta - Part A Mol. Biomol. Spectrosc.* **2015**, 150, 187–189.
- 370 [26] W. H. M. Abdelraheem, X. He, Z. R. Komy, N. M. Ismail, D. D. Dionysiou, *Chem.*
371 *Eng. J.* **2016**, 288, 824–833.
- 372 [27] Y. Ji, Photochemical and photocatalytic degradation of pharmaceutical and personal
373 care products (PPCPS) in aqueous solution: a case study of atenolol and 2-
374 phenylbenzimidazole-5-sulfonic acid, Ph.D., Université Claude Bernard - Lyon I,
375 **2014**.
- 376 [28] Y. Ji, L. Zhou, C. Ferronato, A. Salvador, X. Yang, J.-M. Chovelon, *Appl. Catal. B*
377 *Environ.* **2013**, 140–141, 457–467.
- 378 [29] Y. Ji, L. Zhou, Y. Zhang, C. Ferronato, M. Brigante, G. Mailhot, X. Yang, J.-M.
379 Chovelon, *Water Res.* **2013**, 47, 5865–5875.
- 380 [30] E. De Laurentiis, M. Minella, M. Sarakha, A. Marrese, C. Minero, G. Mailhot, M.
381 Brigante, D. Vione, *Water Res.* **2013**, 47, 5943–5953.
- 382 [31] S. K. Sagoo, R. A. Jockusch, *J. Photochem. Photobiol. A Chem.* **2011**, 220, 173–178.
- 383 [32] R. Cercola, E. Matthews, C. E. H. Dessent, *J. Phys. Chem. B* **2017**, 121, 5553–5561.
- 384 [33] J. V Olsen, B. Macek, O. Lange, A. Makarov, S. Horning, M. Mann, *Nat. Methods*
385 **2007**, 4, 709–712.
- 386 [34] M. J. Frisch, G. W. Trucks, H. B. Schlegel, G. E. Scuseria, M. A. Robb, J. R.
387 Cheeseman, G. Scalmani, V. Barone, B. Mennucci, G. A. Petersson, et al., *Gaussian*
388 *09, Rev. D.01, Gaussian Inc.* **2009**, Wallingford, CT.
- 389 [35] D. Schröder, M. Buděšínský, J. Roithová, *J. Am. Chem. Soc.* **2012**, 134, 15897–
390 15905.
- 391 [36] E. Matthews, C. E. H. Dessent, *J. Phys. Chem. A*, **2016**, 120, 9209–9216.
- 392 [37] S. B. Nielsen, M. B. Nielsen, A. Rubio, *Acc. Chem. Res.* **2014**, 47, 1417–1425.
- 393 [38] A. Henley, H. H. Fielding, *Int. Rev. Phys. Chem.* **2019**, 38, 1–34.

- [39] D. Serxner, C. E. H. Dessent, M. A. Johnson, *J. Chem. Phys.* **1996**, *105*, 7231-7234.
- [40] P. B. Armentrout, *J. Am. Soc. Mass Spectrom.* **2002**, *13*, 419–434.
- [41] Whilst we have not quantitatively calibrated the HCD collision energies used in this experiment, earlier work from our group has established that the 20-38% HCD collision energy range closely correlates to internal energies of ~4-6 eV,^[32] which falls directly into the range of photon energies used within this experiment.
- [42] B. Lucas, M. Barat, J. A. Fayeton, C. Jouvet, P. Çarçabal, G. Grégoire, *Chem. Phys.* **2008**, *347*, 324–330.
- [43] L. A. Baker, B. Marchetti, T. N. V. Karsili, V. G. Stavros, M. N. R. Ashfold, *Chem. Soc. Rev.* **2017**, *46*, 3770–3791.
- [44] A. Alberti, D. Macciantelli, *Spin Trapping. Electron Paramagnetic Resonance*: John Wiley & Sons, Inc.; **2008**, 285–324.
- [45] B. Marchetti, T. N. V. Karsili, M. N. R. Ashfold, *Phys. Chem. Chem. Phys.* **2019**, *21*, 14418-14428.
- [46] R. Losantos, I. Funes-Ardoiz, J. Aguilera, E. Herrera-Ceballos, C. García-Iriepe, P. Campos, D. Sampedro, *Angew. Chem. Int. Ed.* **2017**, *56*, 2632-2635.

TABLES

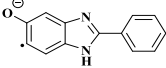
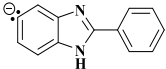
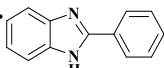
Table 1. Calculated relative electronic energies and gaseous vertical detachment energies (VDE) of the deprotonated isomers of PBSA calculated at the B3LYP/6-31+G** level.

Isomer	Relative Electronic Energy (kJ/mol) ^[a]		VDE (eV) ^[b]
	Gaseous	Acetonitrile	
O14	0	0	4.39
N20	14.3	90.7	4.04

^[a] Zero-point energy corrected.

^[b] VDE = E (neutral at optimized anion geometry) – E (anion). This is included in the table for comparison with the experimental spectra.

Table 2. Proposed structures for the ionic fragments of deprotonated PBSA (m/z 273) produced upon higher-energy collisional dissociation (HCD) and laser photoexcitation.

Ionic Fragment Mass (m/z) ^[a]	Proposed Structure of Fragment	Accompanying Neutral Fragment Lost	Observed in HCD ^[b]	Observed in Laser Photoexcitation ^[b]
208		HSO ₂ •	✓ (vw)	✓ (w)
193		SO ₃	✓ (vs)	✓ (s)
80	SO ₃ ^{•-}		✓ (vw)	✓ (m)

^[a] Determined with mass accuracy > 0.3 amu.

^[b] Very strong (vs), strong (s), medium (m), weak (w), and very weak (vw).

FIGURE CAPTIONS

Scheme 1. Schematic diagram of PBSA with atom labels.

Figure 1. Negative ion electrospray ionization mass spectrum of $[\text{PBSA-H}]^-$ (m/z 273).

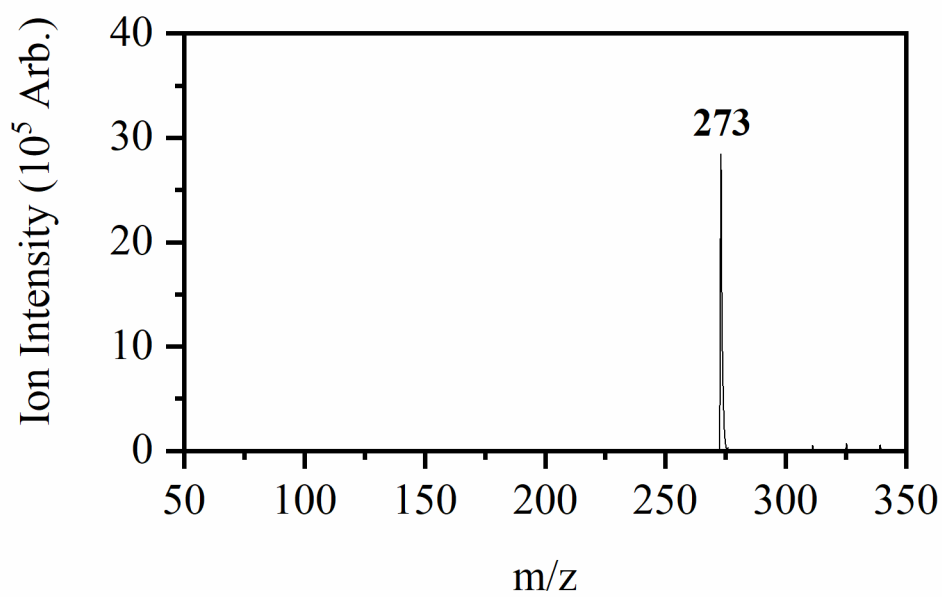
Figure 2. (a) Gas-phase UV absorption (photodepletion) spectrum of $[\text{PBSA-H}]^-$. **(b)** Aqueous UV absorption spectrum of PBSA ($3 \times 10^{-5} \text{ mol dm}^{-3}$) at pH 7.1.

Figure 3. Photofragment difference (laser on – laser off) mass spectra of $[\text{PBSA-H}]^-$, excited at four photodepletion maxima of **(a)** 3.8, **(b)** 4.5, **(c)** 4.9, and **(d)** 5.3 eV.

Figure 4. (a) Gas-phase UV absorption (photodepletion) spectrum of $[\text{PBSA-H}]^-$. **(b-d)** Photofragment production spectra of the three photofragments with m/z 80, 193, and 208, respectively. The solid line is a five-point adjacent average of the data points.

Figure 5. Relative ion yield plots for the m/z 80, 193, and 208 photofragments of $[\text{PBSA-H}]^-$ between 3.25-5.25 eV.

Figure 6. Parent ion dissociation curve of $[\text{PBSA-H}]^-$ along with production curves for the three most intense fragments formed upon HCD between 0-75% energy. The curved lines included with the data points are a five-point adjacent average of such points and are provided as a viewing guide, to emphasize the profile for each individual fragment.



447
448 **Figure 1.**
449

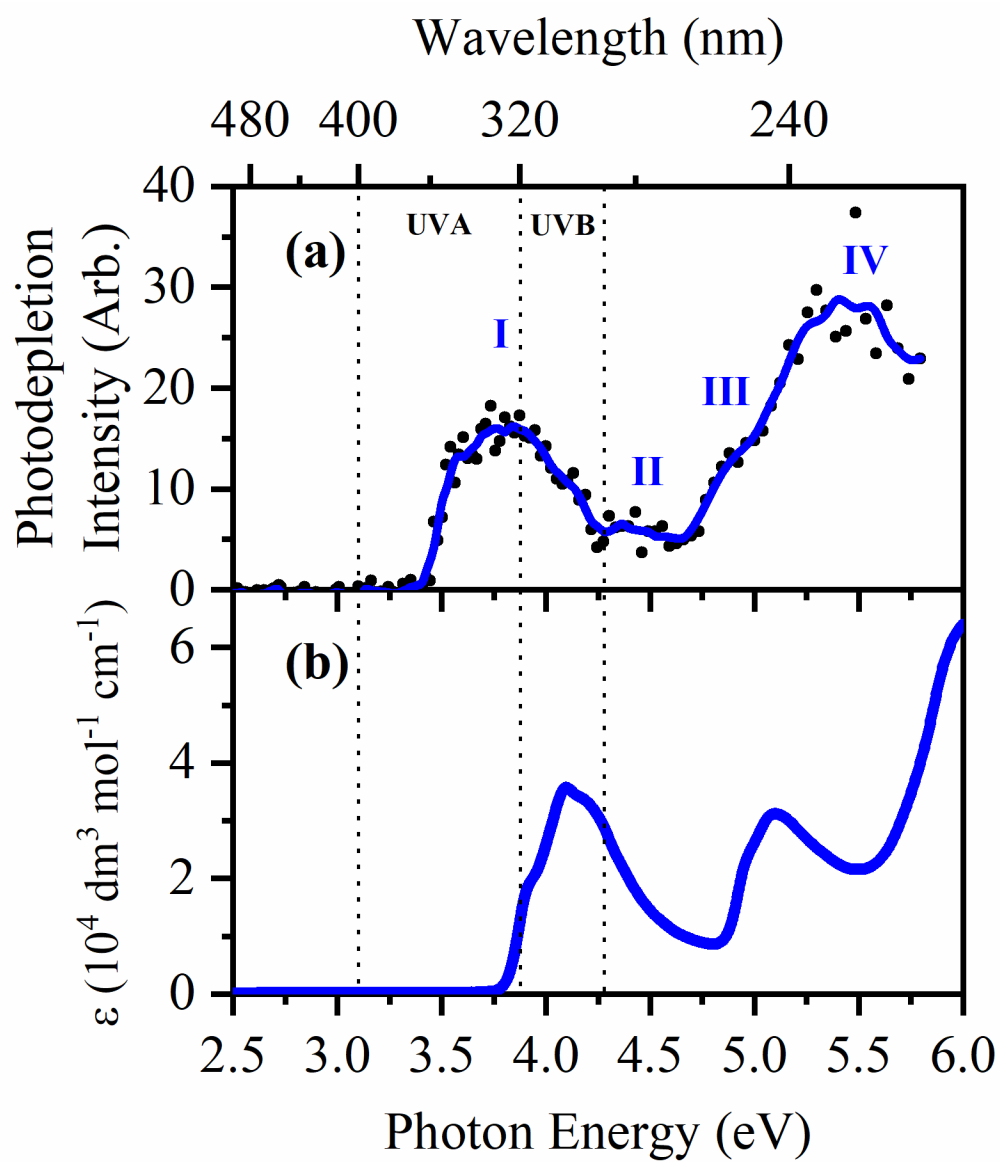


Figure 2.

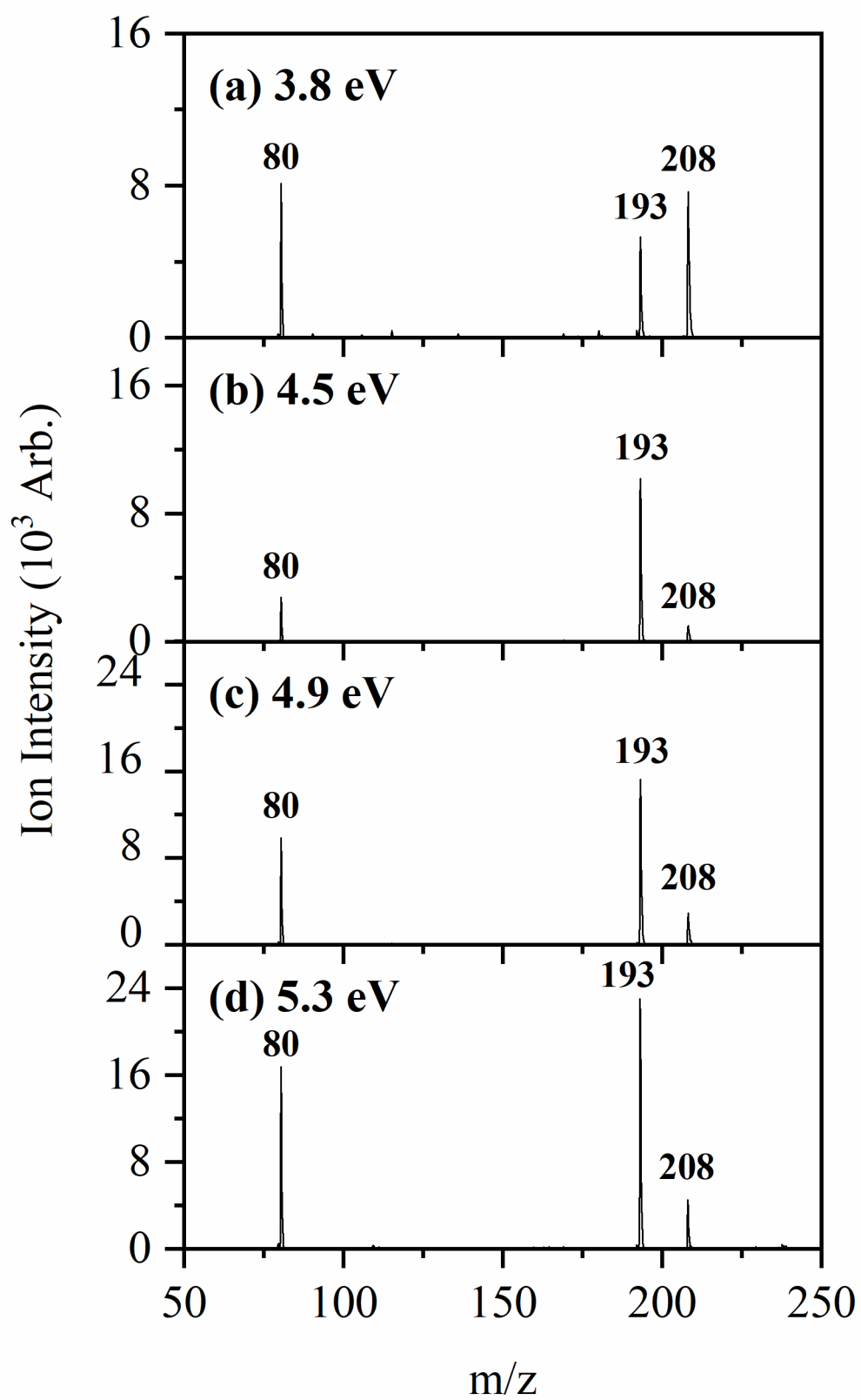


Figure 3.

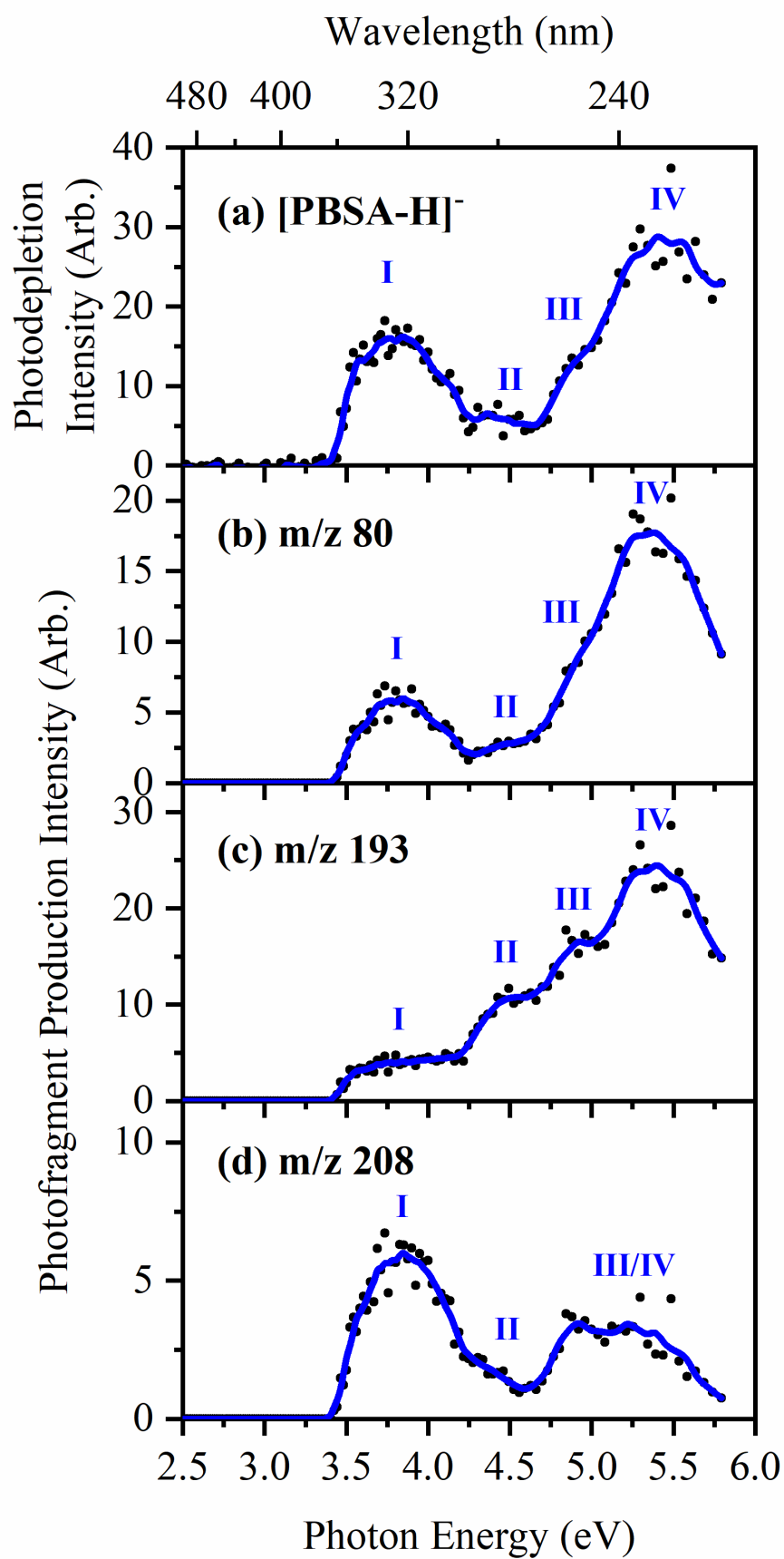


Figure 4.

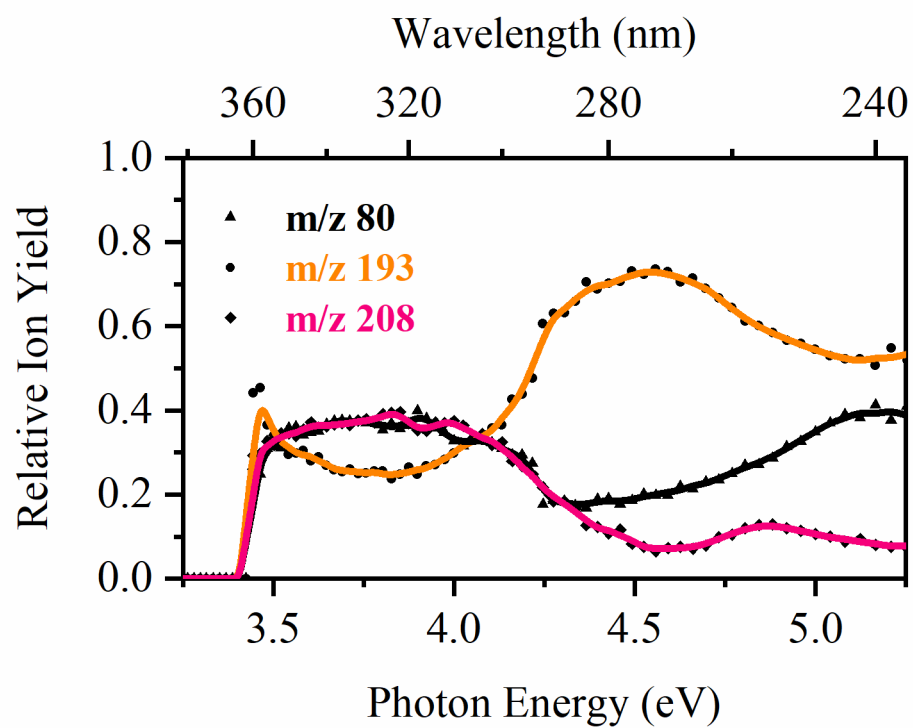
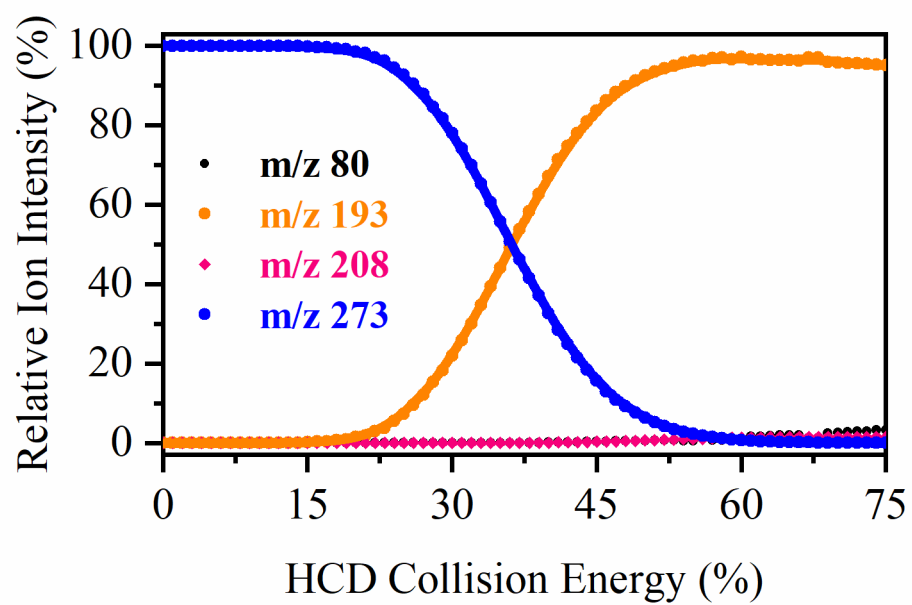


Figure 5.

461



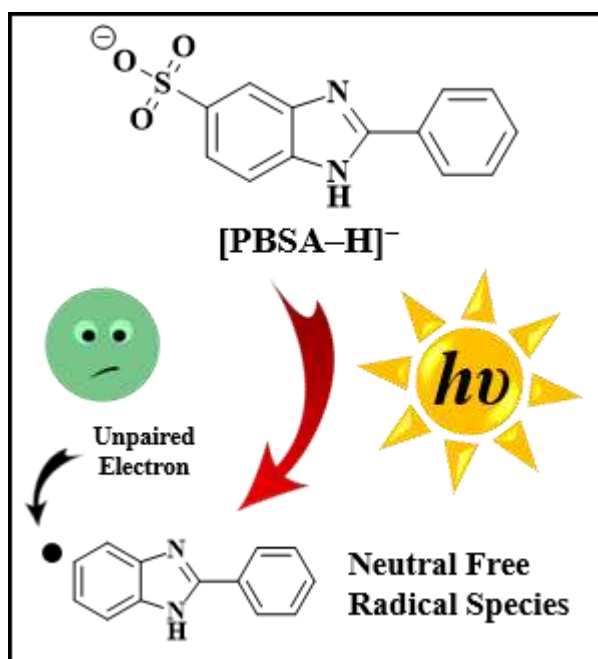
462

463 **Figure 6.**

464

TOC GRAPHICAL ABSTRACT

2-phenylbenzimidazole-5-sulfonic acid (PBSA) is a common UV filter, which is known to exhibit photosensitizing properties. Using novel laser-interfaced mass spectrometry, we directly identify the UV photodegradation products of PBSA, and present evidence that the T_1 state, associated with photosensitization, decays with direct free radical production.



478 **Supporting Information**

479

480 **Direct Observation of Photochemical Free Radical Production from the Sunscreen 2-**
481 **Phenylbenzimidazole-5-Sulfonic Acid via Laser-Interfaced Mass Spectrometry**

482

483 Natalie G. K. Wong, Jacob A. Berenbeim and Caroline E. H. Dessent*

484 Department of Chemistry, University of York, Heslington, York, YO10 5DD, U.K.

485

486 * Corresponding author: Email: caroline.dessent@york.ac.uk

487

488

489

490 S1. Laser Power Measurements

491 S2. Electron Detachment Action Spectra

492

Section S1: Laser Power Measurements

Laser power measurements were conducted on [PBSA-H]⁻ at two photon energies, 3.8 and 5.3 eV, to test for the presence of multiphoton effects. The plots displayed in Figures S1-S2 include measurements of the power dependence of photodepletion, electron detachment (see Section S2), and the m/z 80, 193 and 208 photofragments.

The ln-ln of the data has been plotted and overlain with a pseudolinear fit. The resultant slope is proportional to the number of absorbed photons.¹ The slopes at both photon energies measure less than 1 (see Figures S1-S2 for values). This result indicates that the action response is not multiphoton in nature. Additionally, the pseudolinear slope is less than one over the fitted region and likely indicates saturation of the linear transition.

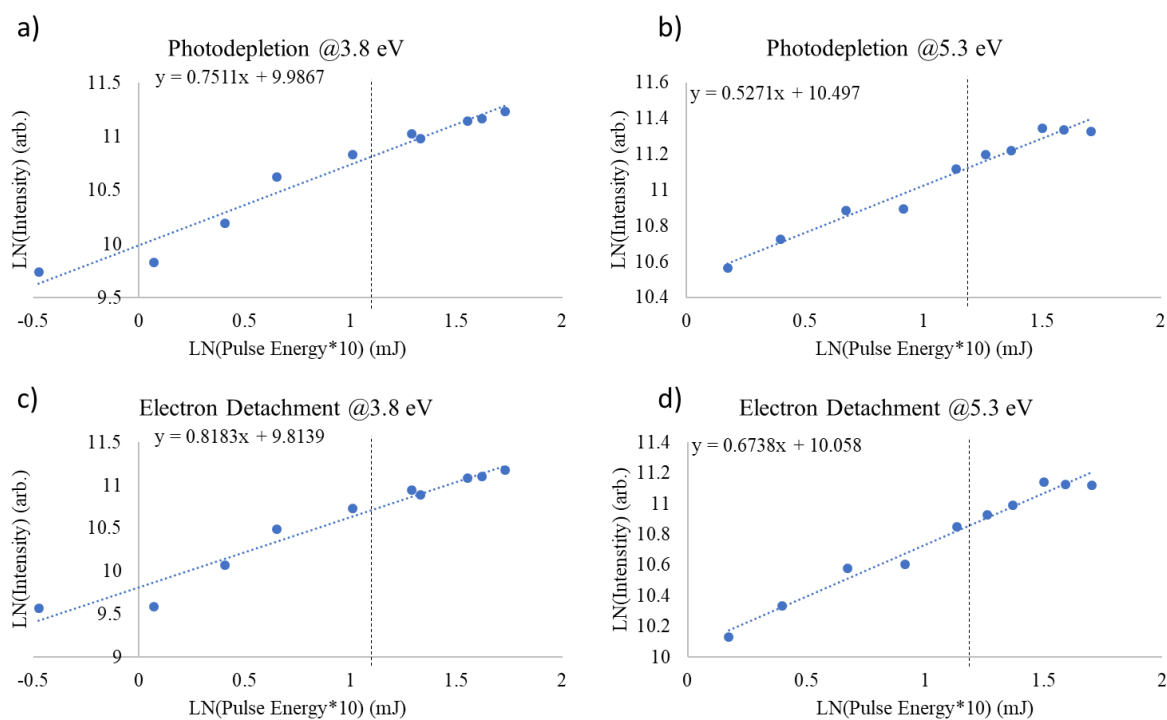


Figure S1 Power Dependence Spectra of photodepletion signal at a) 3.8 eV and b) 5.3 eV and of photoelectron signal at c) 3.8 eV and d) 5.3 eV. Vertical lines indicate pulse energies used during the experiment.

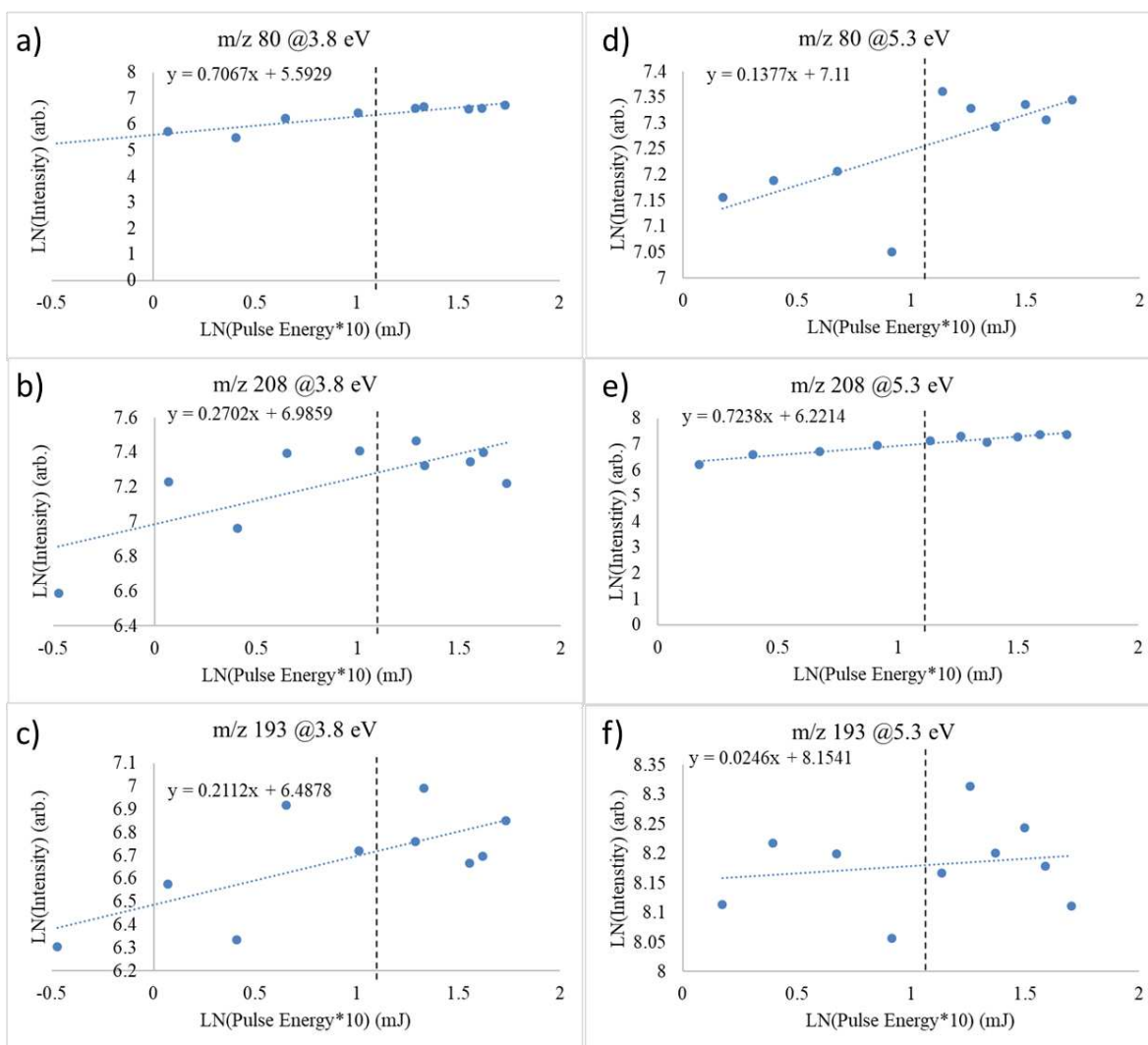


Figure S2 Power Dependence Spectra of ion photofragments m/z 80, m/z 208, and m/z 193 at a-c) 3.8 eV and d-f) 5.3 eV. Vertical lines indicate pulse energies used during the experiment.

Section S2: Electron Detachment Action Spectra

The electron detachment yield of [PBSA-H]⁻ is given in Figure S3. The electron loss is not directly measurable within our instrument, thus these spectra are calculated assuming that any depleted ions that are not detected as ionic photofragments are, instead, losing an electron, i.e. the electron detachment yield = photodepletion ion count – Σ photofragment ion counts. This assumes that both the parent ions and photofragments are detected equally in the mass spectrometer, a reasonable assumption for the systems studied here where the parent ions and fragment ions are reasonably close in *m/z*.

Compared with the photodepletion spectrum displayed in the main text (Figure 2a), the electron detachment yield curve displays a similar profile, indicating that the electron detachment is the main photodepletion pathway. (Note that we have not adjusted the scans presented in Figure S3 by λ (see experimental section), whereas the spectrum in Figure 2a of the main text are. Due to this, the spectral intensity in the higher energy region is moderately reduced in the spectra displayed in Figure S3.)

As discussed in the main text, our calculations indicate that the vertical detachment energy of [PBSA-H]⁻ is ~4.4 eV. From the electron detachment yield spectrum shown in Figure S3, this suggests that electrons are being detached below the VDE for [PBSA-H]⁻. We have seen similar effects in deprotonated adenosine monophosphate anions,^[1] and this observation suggests that upon electronic excitation, the excess electron has access to a pathway that allows it to detach at energies below the VDE.

To give some further information about the relative extent of electron detachment versus ionic fragmentation, Table S1 provides ion counts measured in a typical experimental run conducted in this work. These numbers again show that electron detachment is the major excited state decay channel for gaseous [PBSA-H]⁻ is electron detachment.

[1] R. Cercola, E. Matthews, C. E. H. Dessent, *J. Phys. Chem. B* **2017**, *121*, 5553–5561.

Table S1 Percent electron depletion of [PBSA-H]⁻ calculated directly from precursor ion and ionic photofragment intensities.

		Intensity (ion counts)		
Ion		3.8 eV	4.36 eV	5.5 eV
Precursor	Ion			
Depletion		215362	63784	213055
<i>m/z</i> 80		8105	2150	11960
<i>m/z</i> 193		5298	7946	17991
<i>m/z</i> 208		7665	1586	1598
% electron detachment		90.2	81.7	85.2

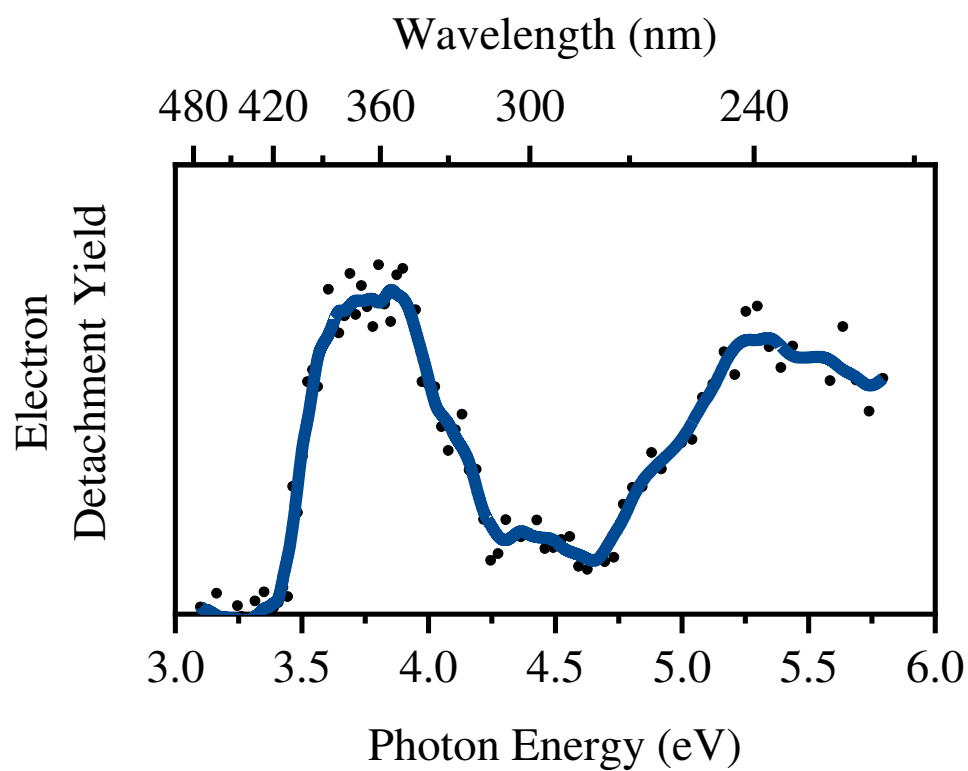


Figure S3 Electron detachment yield of [PBSA-H]⁻. The solid blue lines are five-point adjacent averages of the data points.